J. Fluid Mech. (1994), *vol.* 260, *pp.* 185–209

A numerical and experimental study of transition processes in an obstructed channel flow

By E. P. L. ROBERTS†

Department of Chemical Engineering, University of Cambridge, Pembroke Street, Cambridge, CB2 3RA, UK

(Received 6 June 1992 and in revised form 30 March 1993)

Incompressible Newtonian flow in a two-dimensional channel with periodically placed sharp edged baffles has been studied both by numerical simulation and by experimental flow visualization. The flow was observed to be steady and symmetric at low Reynolds numbers, with recirculating eddies downstream of each baffle. At a critical Reynolds number (based on channel width and cross-sectional mean velocity) of approximately 100 the flow became asymmetric and unsteady. This transition to unsteadiness led to an eddy shedding regime, with eddies formed and shed successively from each baffle. A stability study suggested that the mechanism for transition to unsteady flow is a Kelvin–Helmholtz instability associated with the shear layer formed downstream of the sharp edged baffles. The frequency of the unsteadiness is, however, dependent on the full flow field, and not only the shear layer characteristics. Experimental observations show that the instability is followed by a secondary transition to three-dimensional disordered flow. Experimentally observed flows in the two-dimensional regime were found to be in close agreement with the numerical simulation for both the steady and unsteady flows.

1. Introduction

The transition of a flow from a stable steady state to an unsteady regime can be regarded as the first step towards a fully developed turbulent flow. The nature of this transition may therefore affect both the route taken towards turbulence, and perhaps even the form of the turbulent flow itself. Historically, theoretical studies of this type of transition have centred around classical stability theories (e.g. Lin 1955). Stability theory has developed so that transition processes in some simple (parallel) flows can now be explained using linear and nonlinear stability theory (Orszag & Patera 1983). More recently classical stability and bifurcation theories have been combined with modern numerical flow modelling in order to study transition for flows in more complex geometries. This has led to improvement in the understanding of symmetry breaking properties (Sobey & Drazin 1986) and transition mechanisms (Ghaddar *et al.* 1986; Karniadakis, Mikic & Patera 1988) for flows in engineering geometries. This work has indicated the need for further studies of transition processes for flows in a range of geometries, so that a general understanding of low-Reynolds-number transition can be established. Furthermore, a study which includes experimental observations of how the first transition affects the developing flow will provide further insight into transition mechanisms. Some of the relevant developments in the understanding of transition processes and the use of classical stability and bifurcation theories is outlined below.

† Present address: EA Technology, Environmental Technology Division, Capenhurst, Chester, CH1 6ES, UK.

The stability and symmetry breaking properties of two-dimensional channel flows has been the subject of interest for many years (e.g. Lin 1955). Although the equations describing the stability of simple parallel flows were formulated early this century (in the form of the classical Orr–Sommerfeld equation, Drazin & Reid 1981), accurate numerical solutions to these equations have only been possible in the last thirty years (Orszag 1971). The stability of plane Poiseuille flow has been the subject of detailed study, and has been shown to go through a subcritical Hopf bifurcations at a critical Reynolds number (based on mean velocity and channel width) of order 7700 (Orszag 1971). At this Reynolds number two-dimensional viscous perturbations, known as Tollmien–Schlicting waves (Drazin & Reid 1981), will become unstable and grow with time. This is in sharp contrast to experimental observations which show a transition to a turbulent flow that occurs at a Reynolds number of order 2000 (e.g. Kao & Park 1970). This transition has been explained numerically by Orszag & Kells (1980) who showed that the plane Poiseuille flow with a small amplitude (but finite and stable) Tollmein–Schlichting perturbation can become unstable to infinitesimal three-dimensional perturbations.

In recent years bifurcation theory has been found to be particularly useful for the understanding of flow transitions (e.g. Sobey & Drazin 1986). Two types of bifurcation have been commonly observed in the field of fluid mechanics: the fold and the Hopf bifurcations. A fold bifurcation is a transition from a flow with a single stable state to a flow with two possible stable solutions. A Hopf bifurcation is the transition of a flow from a steady stable regime to an unsteady flow. From a dynamical systems viewpoint, the equations describing the flow of an incompressible Newtonian fluid are a damped nonlinear system under one control parameter (Reynolds number), and would be typically expected to go through either a fold bifurcation or a Hopf bifurcation at some critical Reynolds number (Thompson & Stewart 1986). The fold bifurcation can take a number of different forms (e.g. transcritical, saddle-node), and for a symmetric geometry is expected to be a cusp bifurcation, which is the transition of a symmetric steady flow to a flow with two possible asymmetric steady states. A Hopf bifurcation can take one of two forms: a subcritical Hopf bifurcation, which is typically a transition from a steady state to a nonlinear unsteady flow, and a supercritical Hopf bifurcation, which is a transition from a steady state to a stable unsteady but periodic solution. These bifurcations have been observed for a wide range of geometries, and the transition behaviour of some of the more relevant geometries is discussed below.

A frequently studied geometry is the symmetric sudden channel expansion. The flow in this geometry is experimentally observed to go through a cusp bifurcation from a stable symmetric state to two stable asymmetric states, with the main stream of the flow attaching to one of the walls (e.g. Durst, Malling & Whitelaw 1974). Sobey & Drazin (1986) have studied the bifurcation behaviour of these flows in detail using numerical simulation, and have observed up to seven steady asymmetric solutions. The flow was observed both experimentally and numerically to become unsteady and periodic at a critical Reynolds number of order 150. The numerical observation of two-dimensional periodicity suggests that this second transition is caused by a two-dimensional Hopf bifurcation. Fearn, Mullin & Cliffe (1989), however, have attributed the unsteadiness to a three-dimensional instability, as they were unable to locate the transition using a two-dimensional simulation. This difference may be caused by the periodicity in the model used by Sobey & Drazin (1986).

Notable numerical studies of transition in periodic channel flow include the grooved channel of Ghaddar *et al.* (1986), and the cylindrically obstructed channel studied by Karniadakis *et al.* (1988). Ghaddar *et al.* (1986) observed that the flow in a periodically

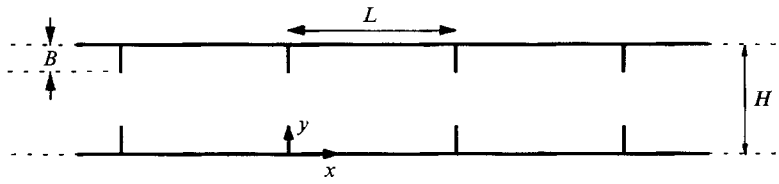

FIGURE 1. The baffled channel geometry.

grooved channel became unstable to two-dimensional perturbations at a Reynolds number of order 1200. This instability was shown to result in a supercritical Hopf bifurcation to a periodic unsteady flow. The perturbation solution was found to be wavelike, with frequency approximately given by the frequency of a Tollmien–Schlichting wave at the perturbation wavelength. This transition was apparently caused by an instability of the shear layer in the groove exciting the stable Tollmien–Schlichting waves in the channel. Karniadakis *et al.* (1988) have studied the stability of a two-dimensional channel flow with periodic cylindrical obstructions. They observed that this flow also went through a supercritical Hopf bifurcation, but at the lower Reynolds number of approximately 125. The frequency was again found to be close to the Tollmien–Schlichting frequency, with the unstable wake flow exciting the stable channel perturbation wave.

This bifurcation of the flow from a steady state to a stable periodic oscillation is common to many different obstructed flows, for example flow over aerofoils, cylinders and other geometries (e.g. Fortin, Fortin & Gervais 1987; Sreenivasan & Strykowski 1987). Oscillations have also been observed in turbulent shear layers and jets (for a review see Ho & Huerre 1984). Clearly bifurcation theory and stability studies can help to provide a deeper understanding of observed asymmetric behaviour (e.g. Sobey & Drazin 1986) and transition mechanisms. The first transition to unsteady flow is also important in engineering terms. From a Lagrangian viewpoint an unsteady flow is fundamentally different to a steady flow, as advected particles are no longer constrained to follow streamlines. This can result in chaotic mixing even for simple flows (Aref 1984), and can have a dramatic effect not only on the mixing rates (e.g. Howes, Mackley & Roberts 1991), but also on heat and mass transfer (Karniadakis *et al.* 1988), filtration (Mackley & Sherman 1992), and particulate processes.

In this paper the flow of an incompressible Newtonian fluid in a two-dimensional periodically baffled channel (see figure 1) is investigated using numerical and experimental techniques. This type of periodically obstructed geometry appears frequently in engineering situations, particularly with heat transfer applications (e.g. Kays & London 1964). Periodic baffles have been used as turbulence enhancers in order to generate the increased heat transfer coefficients observed by Kays & London (1964), and as eddy generators in an oscillatory flow (Brunold *et al.* 1989). In addition to the engineering importance of the geometry, the baffled channel flow is a suitable geometry for a numerical study of stability and transition processes. Stable and unstable steady flows can easily be obtained, owing to the symmetric nature of the geometry. The symmetry of the geometry also allows the definition of a simple perturbation parameter for stability studies and the streamwise periodicity avoids the problems associated with the definition of entry and exit boundary conditions. The presence of a sharp edge ensures that the flow will separate and generate a shear layer at moderate Reynolds number, a common feature of geometries that show an early transition to unsteadiness.

The paper is divided into seven sections. In §2 the theoretical equations and the numerical techniques are described. A description of the experimental flow visualization techniques used is presented in §3. The observed flow patterns are described in §4. In §5 the observed stability behaviour of the numerically obtained flows is described, including a brief study of the base case of plane Poiseuille flow. This section includes the successful estimation of the critical Reynolds number using both linear and nonlinear techniques. An analysis of the transition mechanism for the instability described in §§4 and 5 is presented in §6. The final section is a concluding discussion of the results described in this paper.

2. Theoretical equations and numerical techniques

The geometry studied is a periodically baffled channel as shown in figure 1. With the exception of §5, where the effect of geometric variation on stability behaviour is studied, only one set of values of the geometric parameters has been used. The flow is assumed to be two-dimensional in x and y, and periodic in x.

The fluid mechanics model is in the form of a vorticity – streamfunction finite difference solver for an incompressible Newtonian fluid. The scheme used is based on the work of Sobey (1980) for furrowed channels, and Howes (1988) for ducted tubes. The definition of a streamfunction restricts the model to two spatial dimensions. This model has been used by Howes (1988) to study axisymmetric tube flow, while the results presented in this paper are for two-dimensional channel flow, allowing the relaxation of the centreline symmetry constraint.

In the equations below, length has been made dimensionless with channel width (H), velocities with mean velocity (U), and time with U/H. Vorticity (ω) and streamfunction (ψ) are defined in the usual way:

$$\omega = \frac{\partial v}{\partial x} - \frac{\partial u}{\partial y}, \tag{1}$$

$$u = \left(\frac{\partial \psi}{\partial y}\right), \tag{2}$$

$$v = -\left(\frac{\partial \psi}{\partial y}\right). \tag{3}$$

Where u and v are the dimensionless velocities in the x and y directions, respectively. These definitions lead to Poisson type relationship between ω and ψ:

$$\omega = -\left\{\frac{\partial^2 \psi}{\partial x^2} + \frac{\partial^2 \psi}{\partial y^2}\right\}. \tag{4}$$

From the two-dimensional Navier–Stokes equation and (1), the vorticity transport equation can be derived:

$$\frac{\partial \omega}{\partial t} = -\left(\frac{\partial (u\omega)}{\partial x} + \frac{\partial (v\omega)}{\partial y}\right) + \frac{1}{Re}\left(\frac{\partial^2 \omega}{\partial x^2} + \frac{\partial^2 \omega}{\partial y^2}\right). \tag{5}$$

For the geometry of figure 1 the boundary conditions for these equations are as follows:

(*a*) No slip at the walls: $u = v = 0$ on all walls and baffles; (6)

(*b*) The total volumetric flow rate is equal to the difference in the streamfunction at the top and bottom walls:

$$\text{Top wall:} \quad \psi = 0.5 \sin(2\pi t) \quad \text{for} \quad t < 0.25, \tag{7}$$

$$\psi = 0.5 \quad \text{for} \quad t > 0.25, \tag{8}$$

$$\text{Bottom wall:} \quad \psi = -0.5 \sin(2\pi t) \quad \text{for} \quad t < 0.25, \tag{9}$$

$$\psi = -0.5 \quad \text{for} \quad t > 0.25. \tag{10}$$

The flow is accelerated from rest using (7) and (9), and observed to reach a fully developed steady state at long times. Note that the streamfunction boundary conditions are symmetric in order to avoid the accumulation of asymmetric numerical errors. The flow can be forced to be symmetric by solving one half of the domain of interest and using a centreline boundary condition:

$$\omega = \psi = 0 \quad \text{on the centreline.} \tag{11}$$

Finite difference versions of (2)–(5) form the base equations for the numerical simulation. The vorticity transport equation (5) is used to step forward in time, the Poisson-like equation (4) is then solved for the streamfunction and the velocities are obtained from the definition of streamfunction (2) and (3). The boundary vorticity is obtained using a Taylor expansion of streamfunction away from the wall, and substituting into (4). On the baffles, two values of boundary vorticity are assigned, and at the sharp edge itself, three values are used. This three-value technique was recommended by Roache (1976), but he goes on to conclude that good accuracy at a sharp corner can only be obtained by solving in polar coordinates on a local fine grid centred on the sharp corner. The global flow patterns and the stability behaviour were not found to be sensitive to the treatment of the sharp edge. As the details of the flow close to the sharp edge itself are not the subject of interest in this paper, the three-value technique was thought to provide sufficient accuracy. Centred differencing is used for accuracy and the explicit leapfrog method of Dufort & Frankel (see Roache 1976) is used for the timestepping of the vorticity transport equation. The length of the timestep is chosen to retain numerical stability (based on the convective terms), and typically for these simulations was 0.0025.

The finite-difference equations were solved on a regular grid laid over one cycle of the geometry. The grid size was varied in order to establish a reliable operating regime for the simulation. The total number of grid points was varied from 54 (6×9 grid) up to 10578 (82×129 grid). For both steady and time-dependent flows the observed streamlines were unchanged for grids with more than 1406 points (38×37 grid). In quantitative terms the vortex strength ($2\{\psi_{max} - 0.5\}$) changed by less than 1% for grids with more than 1406 points for a steady flow at $Re = 100$. Similarly for an unsteady flow with $Re = 200$ the growth rate and frequency of the instability (σ, η) both changed by less than 1% for difference grids with more than 1406 points. At a grid size of 33×34 some instability of the vorticity associated with the centred differencing technique is observed close to the sharp edge at $Re = 200$. With a grid size of 42×65 this instability was eliminated. From these observations a grid with 2730 points (42×65) was chosen to give numerical stability without excessive computation time.

Solutions from the simulation with an unbaffled channel ($B = 0$) were compared with the analytical solution of a parabolic velocity profile. The error in the stream

function values was observed to be less than 0.5%. In order to test the accuracy of the time dependence of the simulation a comparison was made with analytical solutions for sinusoidal oscillatory flow in an unbaffled channel. Accurate values of the stream function were obtained with errors again $< 0.5\%$.

The Poisson equation was solved using a multi-grid technique, with residuals solved on successively coarse grids. The spatial periodicity of the flow is achieved numerically by substituting forwards and backwards the conditions at the exit and entry of each cell.

Further details of the numerical techniques and accuracy tests are described by Howes *et al.* (1991) and Roberts (1992).

The stability of the flow is studied using classical perturbation techniques. The basic method for studying the stability of a given flow is described in many modern fluid mechanics text books (e.g. White 1974). Assuming a known steady solution (ψ_s, ω_s) to the flow equations (4) and (5) (with appropriate boundary conditions) has been obtained, a small perturbation (ψ_p, ω_p) is superimposed onto this solution. Thus:

$$\psi = \psi_s + \psi_p, \tag{12a}$$

$$\omega = \omega_s + \omega_p. \tag{12b}$$

In order to determine whether (ψ_s, ω_s) is a stable solution, it is necessary to determine whether a small perturbation will grow or decay with time. The behaviour of finite perturbations can be observed using the solver described above. The perturbation takes one of two forms, depending on the stability of the flow. For stable flows, an artificial perturbation is applied by starting the flow at $t = 0$ with an arbitrary asymmetric flow. Provided the steady symmetric flow is the only stable solution the flow will converge to this stable state. For unstable flows the flow is started with its symmetric solution obtained using the boundary condition (11), and the perturbation is the result of small truncation errors generated by the computer.

The perturbation field (ψ_p, ω_p) can be observed by subtracting the perturbed flow form the initial unperturbed flow:

$$\psi_p = \psi - \psi_s, \tag{13a}$$

$$\omega_p = \omega - \omega_s. \tag{13b}$$

A perturbation amplitude parameter (χ) is chosen as the mean absolute value of the vertical velocity on the centreline:

$$\chi = \frac{1}{L}\int_0^L |v(x, \tfrac{1}{2})| \, \mathrm{d}x. \tag{14}$$

Although a parameter which averages over the whole volume could be used (e.g. the mean sum of the streamfunction on either side of the centreline as used by Sobey & Drazin 1986), χ has been chosen for its physical significance: $\frac{1}{2}\chi L$ is equal to the volumetric exchange rate across the centreline. By observing the behaviour of χ with time for small χ ($\chi \ll 1$) the linear stability behaviour can be studied.

This approach differs from the normal approach to stability studies where the equations for an infinitessimal perturbation are solved independently (e.g. Ghaddar *et al.* 1986). These linear perturbation equations are obtained by substituting (12) into the flow equations ((4) and (5)). Assuming that the perturbation is small products and higher powers of the perturbation terms can be neglected and some terms will cancel from the equations as (ψ_s, ω_s) is known to be a solution. The technique used in this

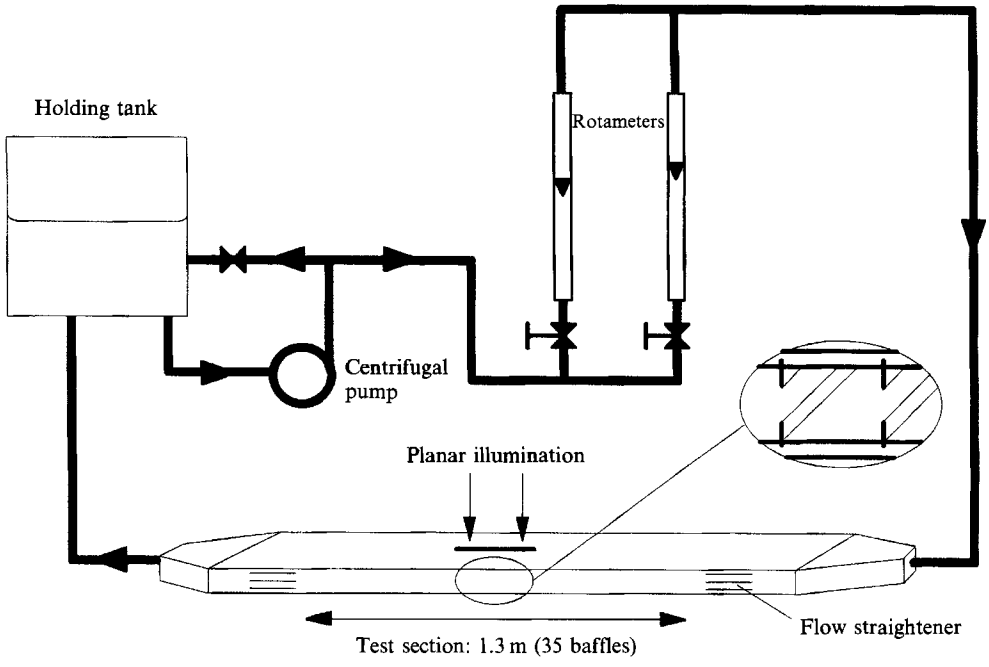

FIGURE 2. Schematic diagram of experimental apparatus.

paper has the advantage that it does not require a separate solver to establish the stability behaviour. This approach is not limited to linear perturbations, as large nonlinear perturbations can also be studied. However, different instability modes cannot be observed, and the limitation to finite-amplitude perturbations makes the absolute stability of a flow difficult to establish.

3. Experimental flow visualization

A diagram of the experimental apparatus is shown in figure 2. The test section consisted of a Perspex channel with periodically placed stainless steel baffles push fitted into the walls. The channel width was 25 mm, with an aspect ratio of 1:8, and a length of 1.3 m (34 baffles). The fluid used was a mixture of methylated spirits and water (60% water, kinematic viscosity 2.535×10^{-6} m^2/s at 20 °C).

Flow was provided by a centrifugal pump and flow loop, with flowrates measured using two calibrated rotameters. From the rotameters the fluid was fed into a 0.4 m length, 50 mm diameter tube fitted with a flow straightener close to the entrance consisting of an array of thin-walled tubes of diameter $\sim$ 3 mm. The tube was also fitted with a flexible diaphragm to reduce any pressure fluctuations generated by the pump. The 50 mm tube was connected to the rectangular channel via a diffuser machined to give a smooth transition from a cylindrical to rectangular geometry. A second flow straightener was positioned in the rectangular channel in order to dampen any disturbances in the entrance region. A 0.2 m unbaffled entrance region was included downstream of the flow straightener.

A mercury vapour lamp was used to provide planar illumination (in the (x, y)-plane) through a narrow slit $\sim$ 3 mm wide at the centreline of the channel. In order to study cross-channel motions a horizontal plane of light (in the (x, z)-plane) just above the centreplane ($y = \frac{1}{2}H$) of the channel was used. Light scattering was achieved with

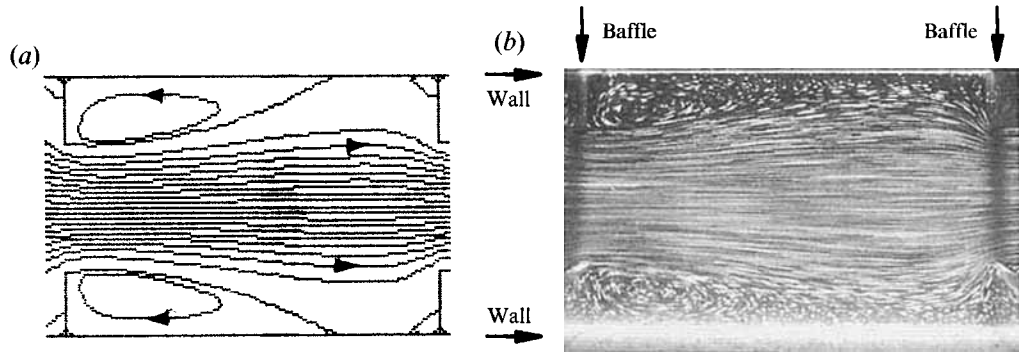

FIGURE 3. Comparison of streamlines and experimental streakline photograph. (*a*) Numerically obtained streamlines. $Re = 60$, ψ at intervals of 0.05, and two extra streamlines to show recirculation. (*b*) Experimental streakline photograph. $Re = 58.5$, Exposure time $= \frac{1}{2}$ s.

neutrally buoyant polyethylene particles having diameter of order 100 μm. Constant volumetric flow was obtained using a centrifugal pump and flow loop, with flowrates measured using a set of rotameters.

The flow patterns were observed using either a video camera or a 35 mm SLR stills camera. Streakline photographs of the flow were taken with exposure times between $\frac{1}{15}$ s and 2 s. Stills taken from the video recordings correspond to an exposure time of approximately $\frac{1}{25}$ s. The streakline photographs reproduced in the paper show the flow patterns observed 18 baffles downstream of the entrance. This should ensure that the flow is fully developed for the range of Reynolds numbers studied in this paper.

4. Observed flow patterns

In this section observed flow patterns for constant volumetric flow in baffled channels are described. The section is divided into two parts. The first describes symmetric flows, obtained numerically using the centreline boundary condition described above. These constrained symmetric flows are compared with the experimentally obtained symmetric flows which occur at low Reynolds numbers. The second part describes asymmetric flows obtained from the simulation, and these flows are compared with experimentally observed asymmetric flows at intermediate Reynolds numbers.

4.1. *Symmetric flows*

Symmetric flow patterns have been obtained from the numerical model using the centreline boundary conditions described above. The flow patterns observed under these conditions are typical of the types of flows observed in obstructed geometries under laminar flow conditions. A recirculating flow is observed downstream of each baffle which grows with Re, as observed for baffled tubes (e.g. Rowley & Patankar 1984; Howes 1988) and in a sudden channel expansion (e.g. Sobey 1985). Under these conditions the flow was observed to reach a fully developed steady state after $t \sim 5$. The observed experimental streakline photographs showed good agreement with the numerical streamlines for Reynolds numbers less than ~ 100. Figure 3 shows a comparison of the numerically observed streamlines with the experimentally obtained streakline photograph for $Re \sim 60$.

Slight asymmetry was observed in the experimental photographs for flows in this regime. This asymmetry was probably due to small geometric asymmetries and

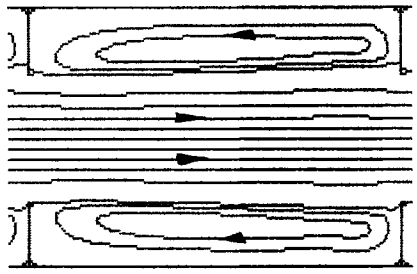

FIGURE 4. Streamlines for constrained symmetric flow with $Re = 300$. ψ at 0.1 intervals, and four extra streamlines to show recirculation.

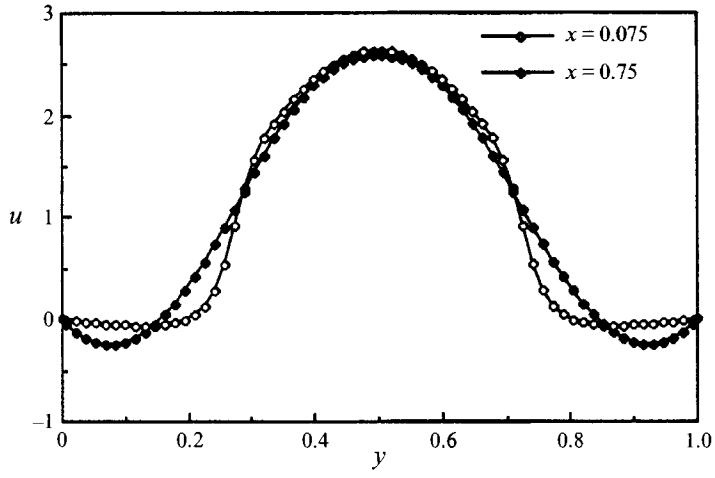

FIGURE 5. Velocity profiles at two different locations. $Re = 200$.

buoyancy effects created by the warmth of the illumination. Video observations showed that the flow in this regime was steady. At the entrance to the test section the flow was observed to require 2–3 cells to become fully developed so that the same flow pattern was observed in each cell.

Figure 4 shows the numerically observed streamlines for the constrained symmetric flow at $Re = 300$. For $Re > \sim 100$ the separated regions occupy most of the inter-baffle space, with the main stream of the flow constrained between the tips of the baffles. This type of flow is reminiscent of a confined planar jet, and is approximately parallel. Figure 5 shows the velocity profiles just downstream of the baffles and midway between the baffles for $Re = 200$. These velocity profiles suggest that the flow is close to a core Poiseuille flow, with the core flow showing an approximately parabolic velocity profile and the inter-baffle region occupied with slow moving fluid. At $Re = 400$ the flow is observed to become unsteady, though the amplitude of the unsteady motion is relatively low. This unsteadiness may be due to either a symmetric instability, a numerical instability generated at high Reynolds numbers close to the sharp edge or it may be an artefact of the numerical simulation.

4.2. *Asymmetric flows*

If the centreline symmetry constraint is relaxed then at a Reynolds number between $Re = 100$ and $Re = 120$ the flow becomes unsteady and periodic, with eddies shed successively from top and bottom baffles. This transition to an unsteady asymmetric

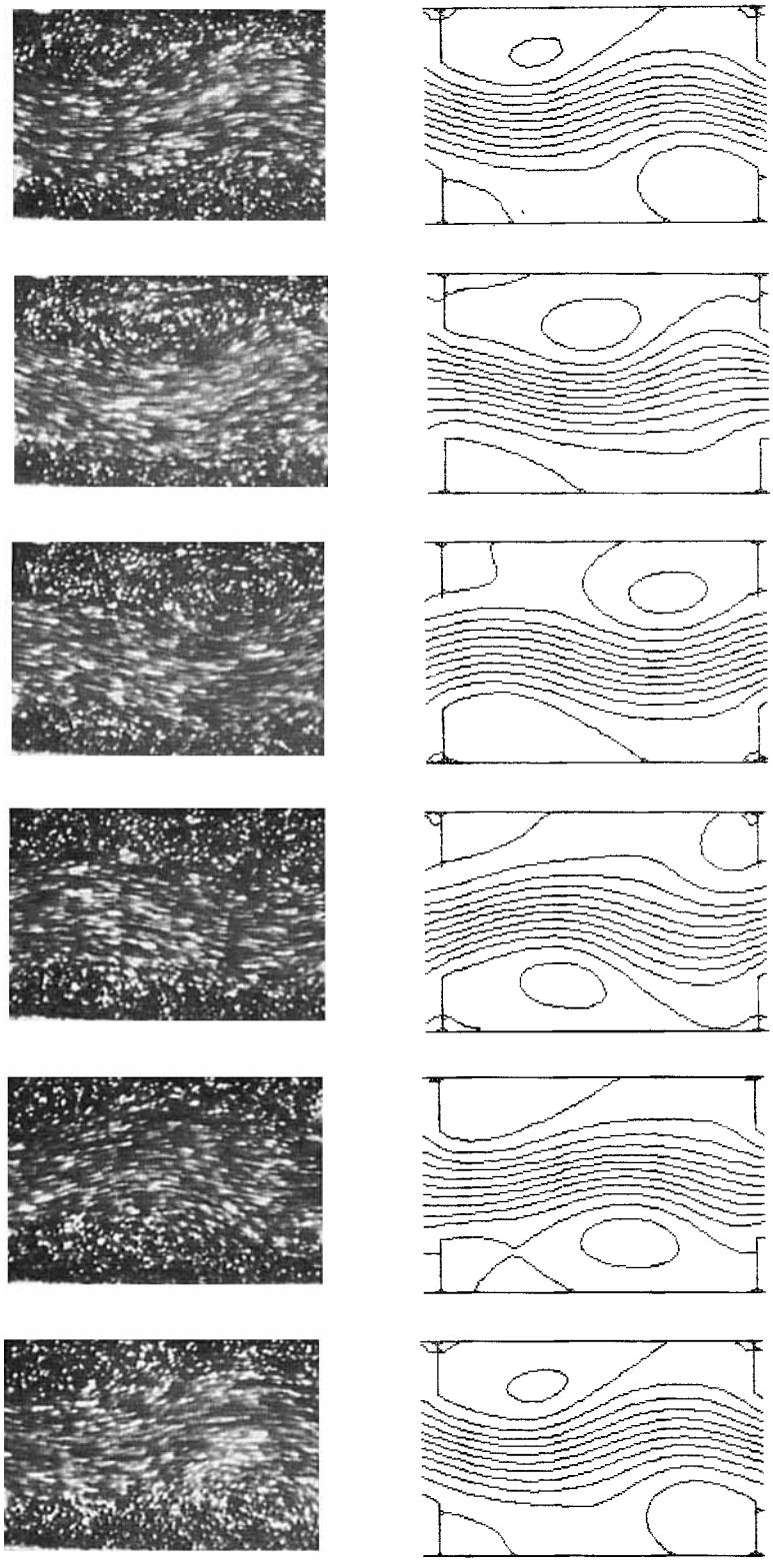

FIGURE 6. Comparison of a sequence of instantaneous streamlines with video frames for $Re = 132$. ψ at intervals of 0.1. Dimensionless time difference between figures = 0.43.

flow has also been observed experimentally at a Reynolds number between $Re = 100$ and $Re = 116$. Figure 6 shows a comparison between the experimentally observed flow patterns and the numerically generated instantaneous streamlines in this asymmetric eddy shedding regime, at $Re = 132$. The experimental streaklines shown have been obtained from a video sequence of the flow. Each picture shows a frame from the sequence at five equally spaced instants in approximately one half period of the flow. The numerically generated streamline sequence was obtained as follows. The streamline patterns were followed for a number of timesteps until the flow patterns corresponded qualitatively with the experimentally observed flow patterns, so that the phase of the oscillation could be established. The sequence of four further plots was then obtained by continuing the simulation for the equivalent dimensionless time intervals as those between each of the video frames. The amplitudes of the asymmetry and the timescale of the unsteadiness show good agreement between the experimental and numerical observations. An approximate dimensionless frequency (Ω, made dimensionless with channel width and the cross-sectional mean velocity) was obtained by frame counting from the video sequence of $\Omega = 0.46 \pm 0.02$ compared with the numerically obtained value of $\Omega = 0.467$.

The experimental flow patterns also show that the flow at the exit of the cell is similar to the flow at the entry to the cell, confirming that a periodic boundary condition is appropriate in this regime. The assumption of periodicity over a single cell was also tested numerically by performing simulations over 2, 6 and 12 cells. No change in the fully developed flow fields was observed.

At Reynolds numbers of order 160 the flow goes through a secondary instability and the observed experimental flow patterns become three-dimensional and disordered. As the numerical model is not capable of predicting three-dimensional flow patterns it is not possible to accurately simulate the fully developed flow patterns in this regime. By accelerating the flow rapidly from rest some comparisons of approximately two-dimensional flows were possible for $Re > 160$. The initially symmetric flows developed large-amplitude asymmetry with periodic eddy shedding before the secondary three-dimensional instability took over and the flow became chaotic. Figure 7 shows a comparison of this large-amplitude asymmetric flow for $Re = 244$ with the numerical streamlines obtained for $Re = 250$. As in figure 6 the experimental figures are frames from a video sequence corresponding to approximately one half cycle of the flow, and the numerical flow was followed until the two were qualitatively in phase. The asymmetry in the experimental flow is still developing and has not reached the level observed using the simulation. The form of the flow patterns, and the timescale of the eddy shedding show good agreement. These observations suggest that the flows shown in figure 7 are dominantly two-dimensional (i.e. in agreement with the numerical simulation of the two-dimensional Navier–Stokes equations). The fully developed two-dimensional flow, however, is unstable in the three-dimensional geometry, and the flow becomes disordered.

At higher Reynolds numbers the level of asymmetry in the solution generated by the numerical model increases. Figure 8 shows observed instantaneous streamlines obtained from the numerical simulation for $Re = 200$, 300 and 400. For $Re \geqslant 400$ the flow was observed to become aperiodic, but it is not clear whether these flows are chaotic, quasi-periodic or transient. This transition at high Reynolds numbers may have been caused by a numerical instability at the sharp edge of the baffles, or by the instability of the symmetric flow mentioned above.

Figure 9 shows a streakline photograph for the fully developed flow at $Re = 198$. The flow is clearly different at the two ends of the cell, and the crossed streaklines

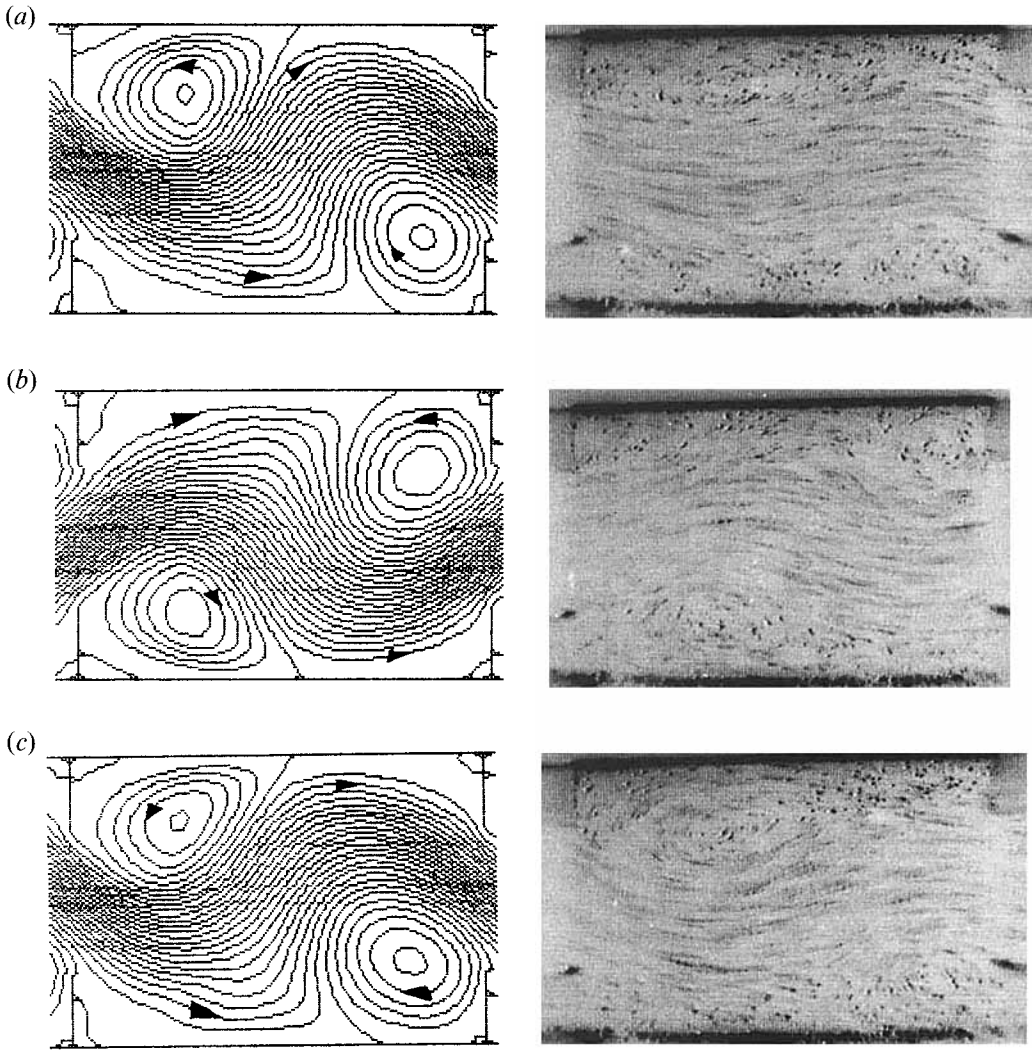

FIGURE 7. Comparison of a sequence of instantaneous streamlines with video frames. ψ at intervals of 0.05. (*a*) $t = t_0$. (*b*) $t = t_0 + 0.95$. (*c*) $t = t_0 + 1.9$.

suggest that the flow may be three-dimensional. Video observations of the flow in this regime show eddy shedding behaviour from both baffles. However, the eddy size varies considerably and the flow shows no periodicity. A streakline photograph for $Re = 359$ is shown in figure 10. The flow appears to be wavelike, with a wavelength of two cells. The main stream of the flow sweeps across the bottom wall, while in adjacent cells the flow appears to sweep across the top wall. Video observations of the flow in the regime $250 < Re < 450$ show that this stationary wavelike flow tends to persist for some seconds, after which the wave swaps over to the opposite wall. While the main stream of the flow sweeps across one wall eddies are rapidly shed from the opposite baffle.

Figure 11 shows a streakline photograph at $Re = 537$. Again the mainstream of the flow sweeps across the bottom wall. Video observations at this Reynolds number show a standing wave is observed in the channel with a wavelength of two cells. This

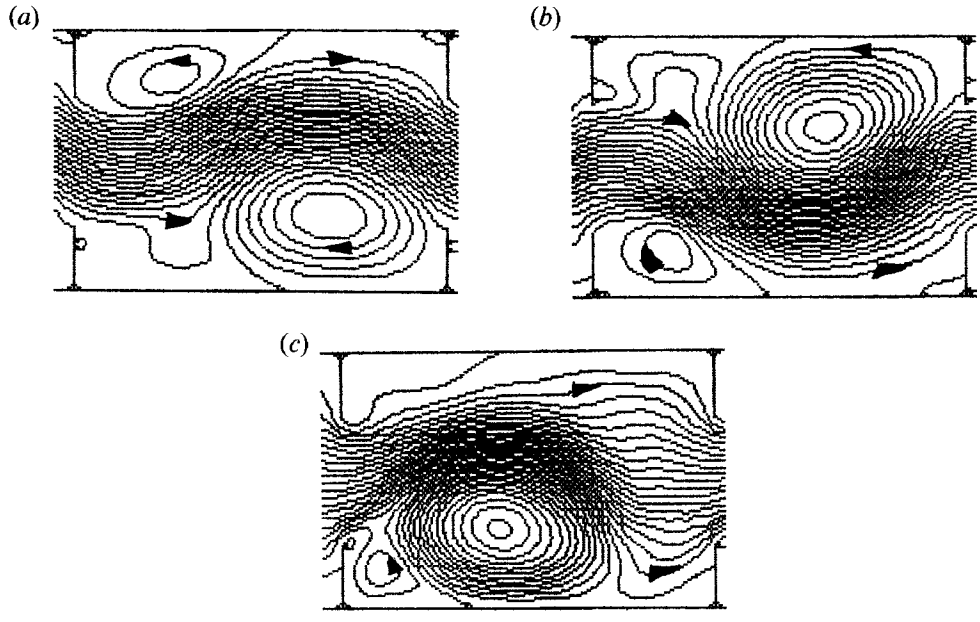

FIGURE 8. Instantaneous streamlines for asymmetric flows. (*a*) $Re = 200$. (*b*) $Re = 300$. (*c*) $Re = 400$.

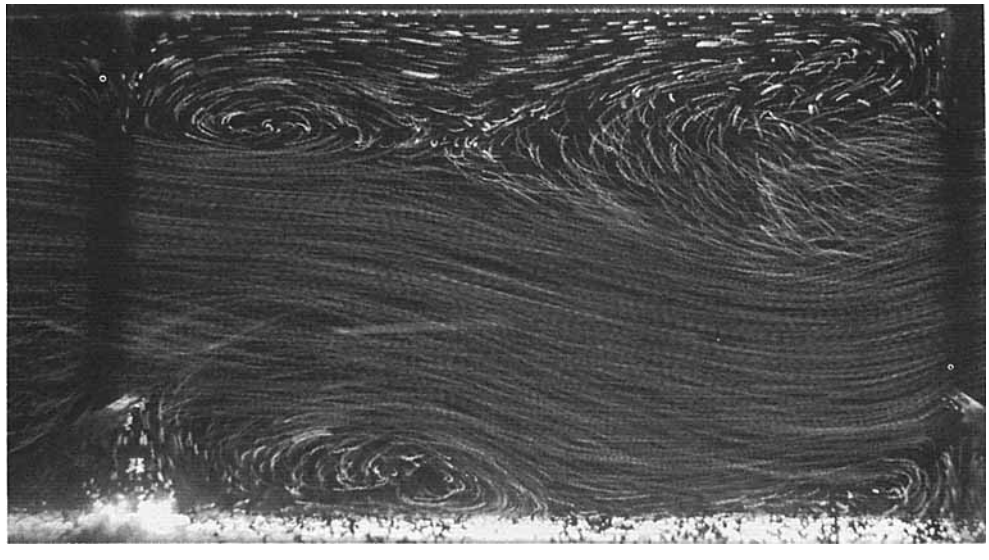

FIGURE 9. Experimental streakline photograph for $Re = 198$. Exposure time = $\frac{1}{8}$ s.

wavelike structure was observed to be very stable, remaining for long periods despite the chaotic nature of the surrounding flow. This effect may be similar to the Coanda effect that has been observed in geometries with a flow expansion (e.g. Durst *et al.* 1974).

In order to establish the three-dimensional nature of the flow the cross-channel motion has been observed for a range of Re. The streakline photograph of the flow viewed from above at $Re = 100$ when the flow is steady, and at $Re = 130$ when the flow

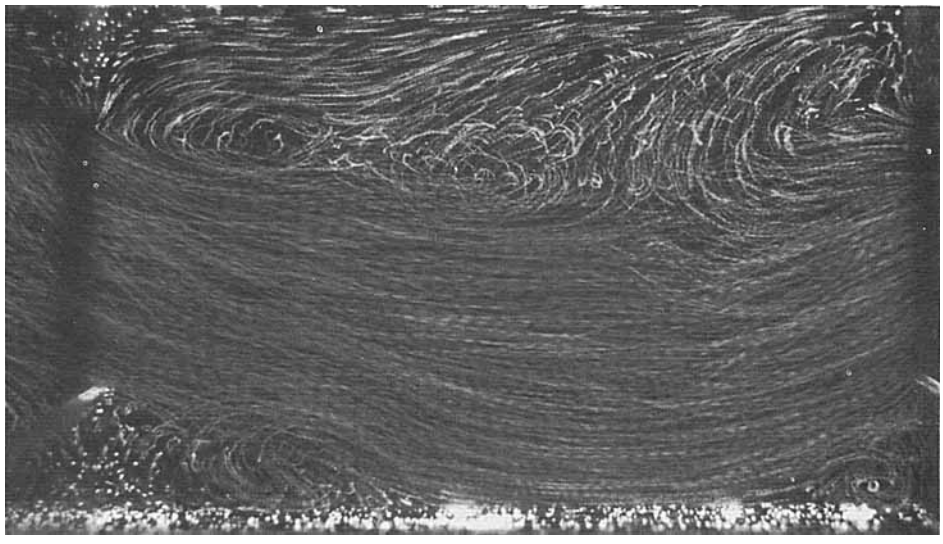

FIGURE 10. Experimental streakline photograph for $Re = 359$. Exposure time $= \frac{1}{8}$ s.

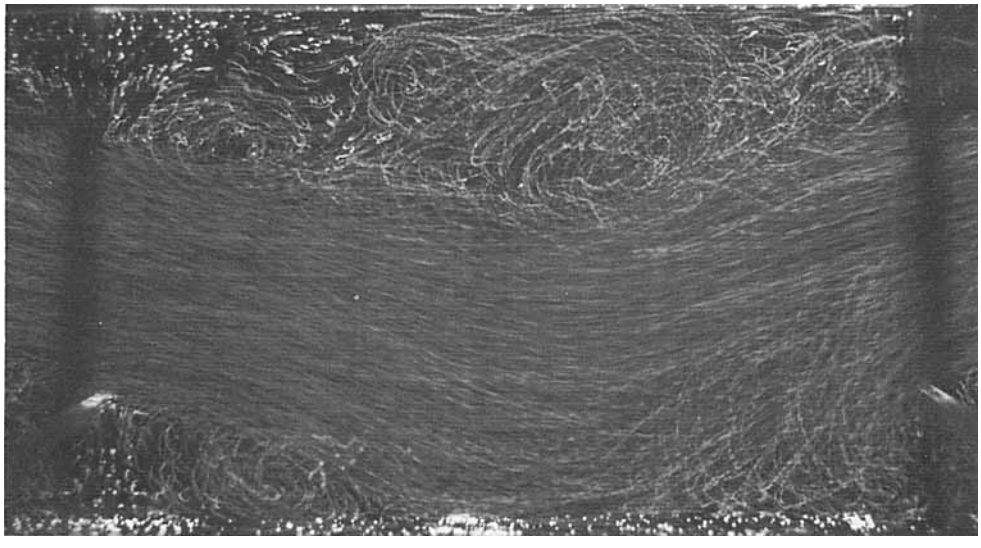

FIGURE 11. Experimental streakline photograph for $Re = 537$. Exposure time $= \frac{1}{8}$ s.

is unsteady and periodic are shown in figures 12 and 13, respectively. Little cross-channel motion is apparent in either figure, confirming that the flow can be considered as two-dimensional in this regime. Figure 14 shows the equivalent streakline photograph at $Re = 160$. Some cross-channel motion is clearly apparent, indicating that the flow has become three-dimensional. At $Re = 300$ (figure 15) the cross-channel motion has developed into a highly complex flow regime.

5. Observed stability behaviour

This section describes the observed stability behaviour of the symmetric flows described above. The section is divided into three parts. A brief assessment of the

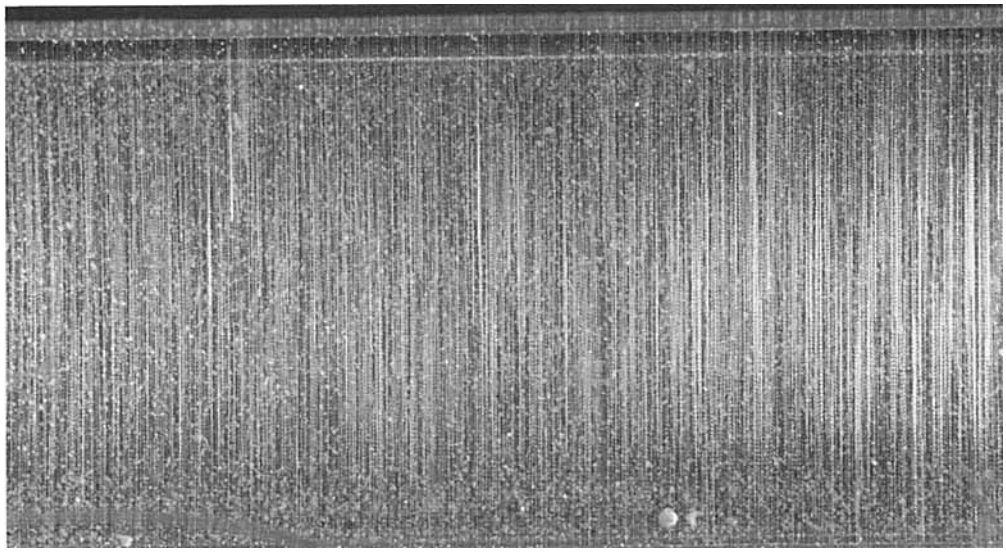

FIGURE 12. Experimental streakline photograph showing cross-channel motion for $Re = 100$. Exposure time $= \frac{1}{2}$ s.

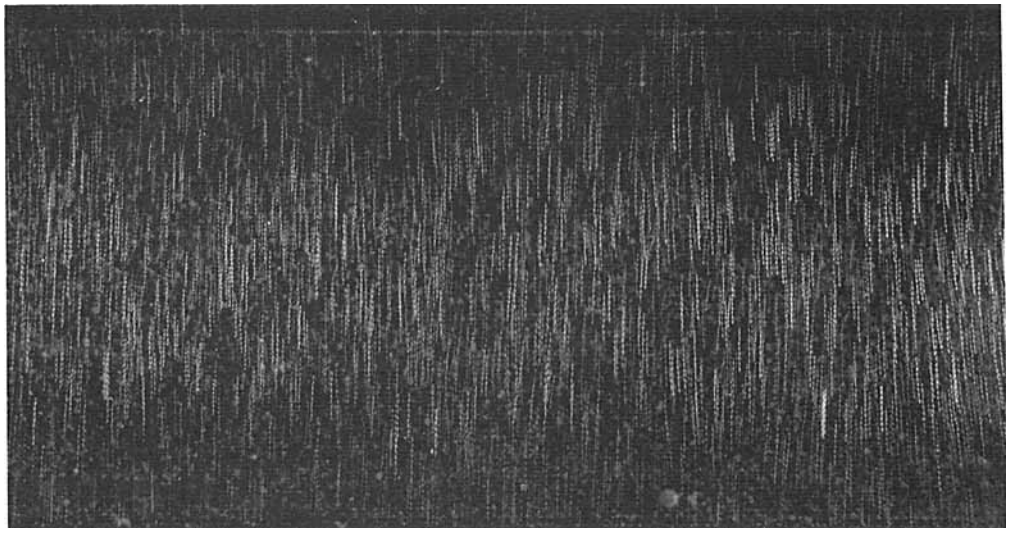

FIGURE 13. Experimental streakline photograph showing cross-channel motion for $Re = 130$. Exposure time $= \frac{1}{15}$ s.

expected perturbation behaviour is outlined below. This is followed by a test of the stability techniques described in §2, using the well-established case of an unbaffled channel. The third section describes the observed stability behaviour for the baffled channel flow.

5.1. *Expected perturbation behaviour*

The symmetric steady flows described above for $Re \geqslant 100$ were observed to be approximately parallel. The behaviour of linear perturbations to parallel flows have

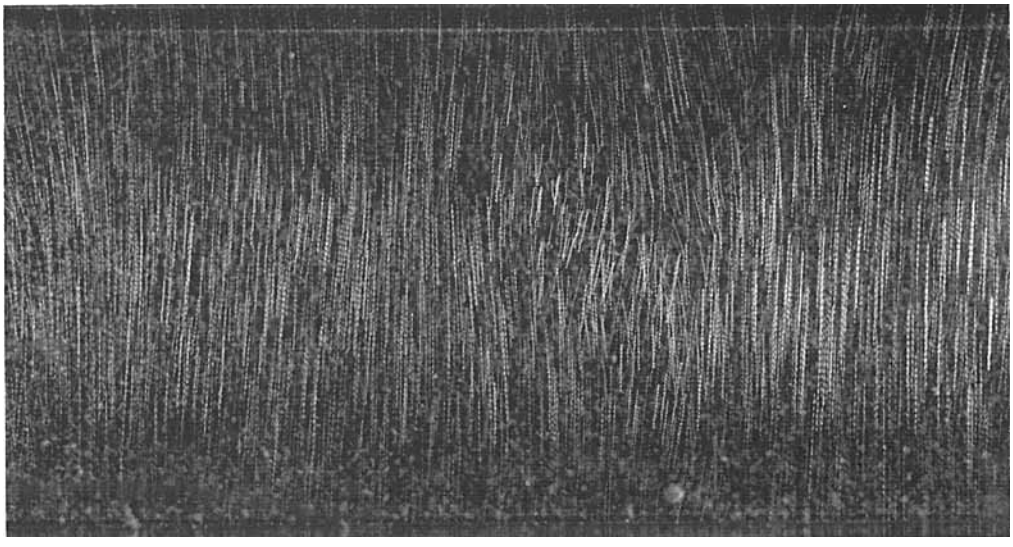

FIGURE 14. Experimental streakline photograph showing cross-channel motion for $Re = 160$. Exposure time $= \frac{1}{8}$ s.

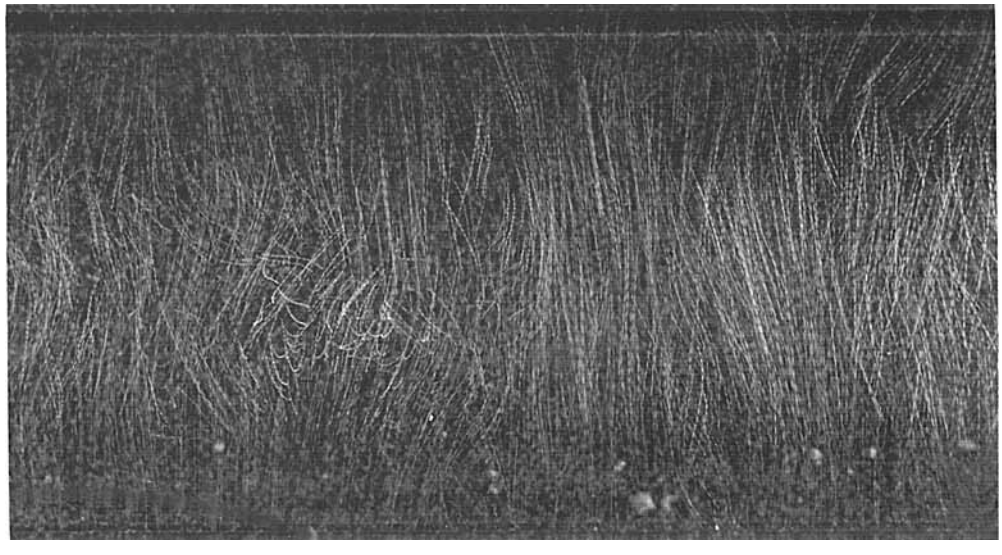

FIGURE 15. Experimental streakline photograph showing cross-channel motion for $Re = 300$. Exposure time $= \frac{1}{2}$ s.

been studied in detail (e.g. Lin 1955) and may give an insight into the stability behaviour of this more complicated geometry. The observations of Ghaddar *et al.* (1986) and Karniadakis *et al.* (1988) have shown that perturbations to obstructed channel flows show many similarities with the stability behaviour of parallel flows.

The stability equations for a parallel flow can be reduced to a single equation known as the Orr–Sommerfeld equation (Drazin & Reid 1981). Solutions to this equation are usually assumed to be of the form

$$\psi = \mathrm{Re}\{\psi_f(y) \exp(\mathrm{i}\alpha x - \mathrm{i}ct)\}, \tag{15}$$

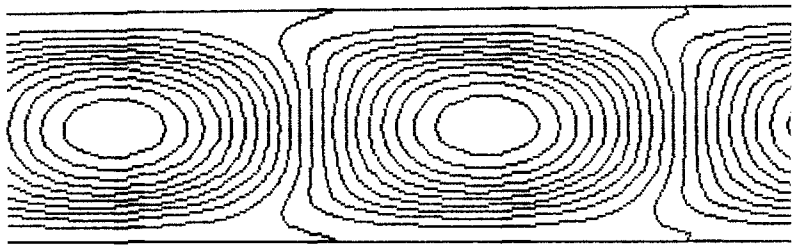

FIGURE 16. Instantaneous perturbation streamlines for a plane channel, $Re = 700$, $L = 3.33$.

where Re{ } is the real part, $\psi_f \alpha$ and c may be complex (Drazin & Reid 1981). In this paper the flow is periodic in x, so that α is real, and the flow was observed to become unsteady so c may be complex:

$$c = \eta + i\sigma. \tag{16}$$

Thus α is the wavelength, η the frequency and σ the growth rate of the instability. The stability analysis can be treated as an eigenfunction (ψ_f) eigenvalue (c) problem. For a given flow, Reynolds number, and wavelength (α), a perturbation function (ψ_f) and associated frequency and growth rate (c) can be obtained. If a flow is stable then all values of σ are negative for all values of α.

Thus if the flow is approximately parallel a perturbation of the form of (15) and (16) may be expected, and χ will grow or decay exponentially in time. A perturbation of the form of (15) and (16) will be wavelike, and a wavelike structure has been commonly observed for obstructed channel flows (Ghaddar *et al.* 1986; Karniadakis *et al.* 1988; Ralph & Pedley 1988).

5.2. *Plane channel flow*

The two-dimensional stability of plane channel flow is now fairly well understood, and accurate solutions to the perturbation equations have been reported in the literature (Orszag 1971). As this is a limiting case of the geometry studied in this paper (with $B = 0$) it is an appropriate geometry to use as a test case for the numerical techniques used for the stability study.

The flow in the plane channel was accelerated from rest to $Re = 700$ and observed to reach a fully developed steady state, close to the known solution of Poiseuille flow. Once the flow has reached a fully developed state an arbitrary asymmetric perturbation is added, and the value of χ was observed to decay. When χ has become small the asymmetric part of the flow should converge to the least stable solution to the Orr–Sommerfeld equation. A wavelength of $L = 3.333$ (Ghaddar *et al.* 1986) was used as this is the least stable wavelength (largest value of σ) at this Re, ensuring that all shorter wavelengths will decay more rapidly. A plot of the perturbation stream function when χ is small is shown in figure 16, which compares very well with the accurate solution given by Ghaddar *et al.* (1986, their figure 4). The value of χ is observed to decay exponentially, with a decay rate (σ) of 0.210, close to the accurate value given by Ghaddar *et al.* (1986) of 0.209. The frequency of the perturbation (η) can also be obtained by observing the behaviour of the perturbation velocity (v_p) at a point on the centreline (this is easily obtained as $v_p = v$ on the centreline). A value of η of 0.165 was obtained, again close to the accurate value (from Ghaddar *et al.* 1986) of 0.164.

These observations indicate that perturbation techniques used with the numerical model are adequate for the study of transition in two-dimensional flow.

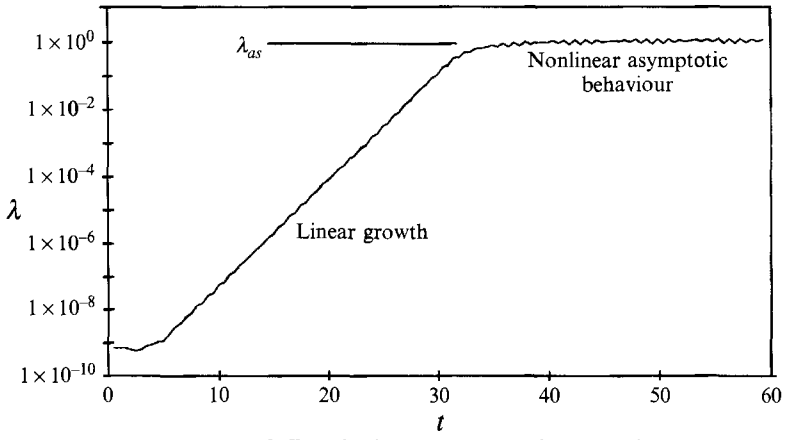

FIGURE 17. Developing asymmetry for $Re = 200$.

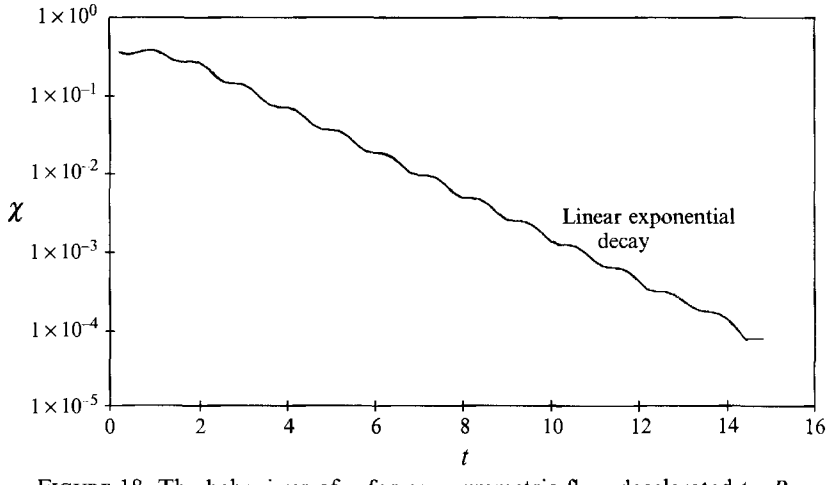

FIGURE 18. The behaviour of χ for an asymmetric flow decelerated to $Re = 60$.

5.3. *The baffled channel*

Starting with symmetric flow in the baffled channel the symmetry constraint is then relaxed, and the value of χ followed in time. If the flow is unstable asymmetric perturbations generated by truncation errors in the program will grow in time, and thus χ will increase. Figure 17 shows the behaviour of χ observed at $Re = 200$. As expected, an exponential behaviour was observed while $\chi \ll 1$, and a value for σ at each unstable Re could be obtained. When the perturbation becomes large (χ of order 1) nonlinear effects take over and χ approaches an asymptotic value. In order to obtain the value of σ for stable flows the decay of an initial perturbation was observed. This was achieved by decelerating an unstable flow to the chosen stable Re once the value of χ has reached ~ 0.1. The unstable perturbation at the higher Re should approximately correspond to the least stable mode at the stable Re. Figure 18 shows the observed behaviour of χ once the flow has been decelerated to $Re = 60$. In this case an exponential decay has been observed and the value of σ can thus be obtained. In figure 19 σ is plotted against Re, and a critical Re for instability (σ positive) of 100–110 has been obtained.

Figure 20 shows the growth of the perturbation velocity at a point on the centreline

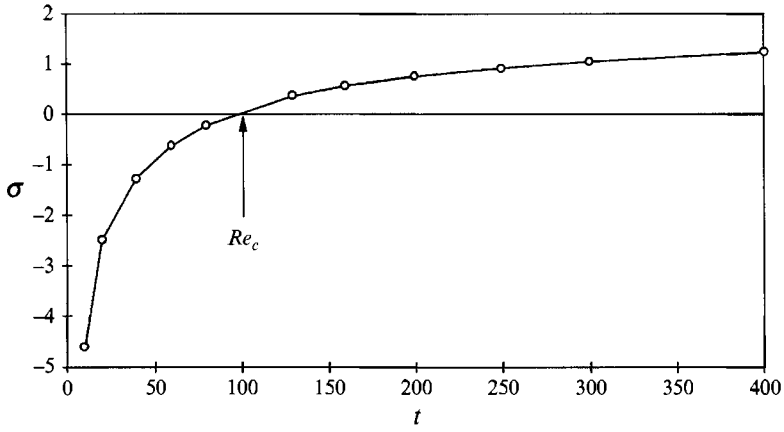

FIGURE 19. Instability growth rate versus Reynolds number.

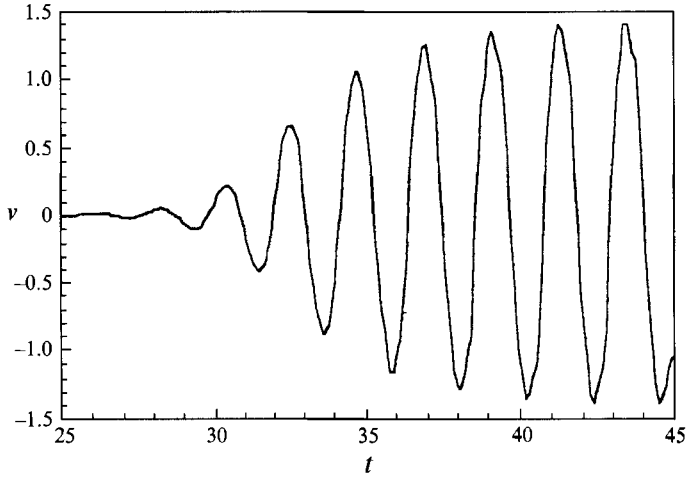

FIGURE 20. The growing oscillation of the perturbation velocity at a point on the centreline for constant volumetric flow, $Re = 200$.

for $Re = 200$. The growing unsteady oscillation suggests that the instability is due to a super-critical Hopf bifurcation. The expected nonlinear behaviour for this type of bifurcation is a self-sustained oscillation (as observed in figure 20) with the amplitude of the oscillation proportional to $(Re - Re_c)^{\frac{1}{2}}$, where Re_c is the critical Reynolds number.

To observe the nonlinear behaviour of the unstable flows χ is observed to grow until exponential behaviour is no longer observed (for $\chi \sim 0.1$). An asymptotic behaviour is observed for long times (see figure 17), and the asymptotic value of χ (χ_{as}) is a measure of the amplitude of the self-sustained oscillation. The value of χ_{as} has been obtained for a range of Re, and a curve of the form of equation 17 fitted to the points,

$$\lambda_{as} = A(Re - Re_c)^{\frac{1}{2}}. \tag{17}$$

Using fitting parameters A and Re_c an excellent fit is obtained (see figure 21). A critical Reynolds number for asymmetry of 101 is obtained, in agreement with the linear analysis and the experimental observations.

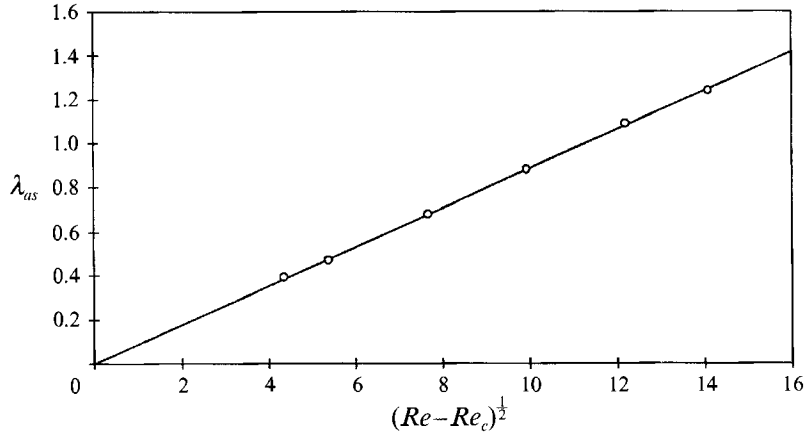

FIGURE 21. Asymptotic level of asymmetry versus root criticality.

6. The transition mechanisms

In order to establish the mechanism for the transition to unsteady flow the perturbation streamlines, the frequency of the instability and the effect of varying the geometry have been studied. Stability theory dating back to 1896 (Rayleigh 1945) has shown that in the limit of vanishing viscosity a parallel flow is stable if the velocity profile has no point of inflexion. The instability of plane Poiseuille flow cannot be explained using inviscid theory, and it is conversely the viscosity of the fluid that is responsible for the observed instability (Drazin & Reid 1981). It is desirable to establish whether the observed instability in the baffled channel flow is caused by a viscous or by an inviscid instability. Viscous instabilities are commonly associated with Tollmien–Schlichting waves, which occur in the presence of a wall. Inviscid instabilities are associated with a point of inflexion in the velocity profile, normally in a shear layer.

Figure 22 shows the perturbation streamlines at $Re = 40$ (stable) and $Re = 200$ (unstable). These are obtained by subtracting the value of the streamfunction for the constrained symmetric flow (equation (13)) at each grid point from the value obtained when χ is small. Only the symmetric perturbation streamfunction is plotted as antisymmetric perturbations were observed to be stable for all flows in this regime (up to $Re = 400$). The wavelike perturbation shown in figure 22 is very similar to the wavelike instability observed by Ghaddar *et al.* (1986) for a periodically grooved channel and Karniadakis *et al.* (1988) for a periodically cylindrically obstructed channel. These workers observed that the frequency of the instability wave was approximately equal to the frequency of the least stable Tollmien–Schlichting wave for plane channel flow. This observation suggests that an instability in the shear layer is exciting the stable Tollmien–Schlichting waves in the channel. Thus the transition is generated by the inviscid instability in the shear layer, while the frequency of the instability is controlled by the viscous Tollmien–Schlichting waves. The frequency of the waves observed in figure 22 are $\eta = 0.46$ for both $Re = 40$ and $Re = 200$. This is not in agreement with the Tollmien–Schlichting frequency for the plane channel flow of ~ 0.68 (for a wavelength equal to the baffle spacing). Nor does the frequency compare with the Tollmien–Schlichting frequencies for the core Poiseuille flow. These observations are not altogether surprising as the baffles have clearly resulted in a very different flow from plane Poiseuille flow. The flows studied by Ghaddar *et al.* (1986)

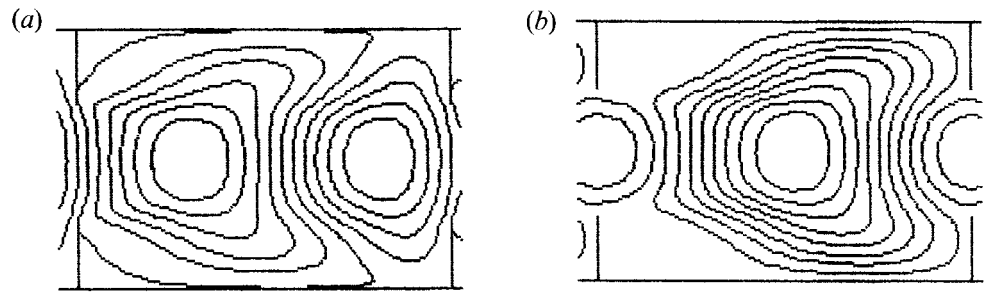

FIGURE 22. Instantaneous perturbation streamlines. (*a*) $Re = 40$, (*b*) $Re = 200$.

and Karniadakis *et al.* (1988) represented only a small perturbation from plane channel flow.

The instability of a planar jet in a stationary fluid has been successfully modelled using inviscid theory (e.g. Sato 1961). The constrained symmetric flow (figure 4) was observed to be similar to a planar jet flow, and the transition of the flow may be related to the transition behaviour of a jet flow. If we consider varying the baffle height (B) then the flow may be considered to be between two extremes:

(i) As B/H (see figure 1) approaches 0 the baffles will represent a small perturbation from plane Poiseuille flow. The frequency of the instability should tend towards the frequency of the least stable Tollmien–Schlichting wave (cf. Ghaddar *et al.* 1986; Karniadakis *et al.* 1988).

(ii) As B approaches $\frac{1}{2}H$ the flow tends towards a planar jet in a stationary fluid, with the walls having little effect.

The stability behaviour of a plane jet has been shown to depend on the velocity profile (Sato 1961), with the instability wave normally observed to travel at the velocity at the point of inflexion in the velocity profile. Sato (1961) has shown that a sinuous plane jet instability is commonly less stable than a varicose instability, in agreement with the observations for the baffled channel flow. Betchov & Criminale (1967) have shown that the presence of a confining wall will reduce the wave speed below the velocity at the point of inflexion. The frequency of the instability wave at $Re = 200$ has been established for a range of baffle heights corresponding to flow area constrictions of $\xi = 2B/H \times 100\% = 12.5$, 25, 32.5, 50, 62.5, 66.75 and 75%. At baffle constrictions with $\xi > 50\%$ grid refinement tests were performed to ensure numerical accuracy. For the largest two baffle heights ($\xi = 66.75\%$ and 75%) a refined grid of 42×128 points was required.

The wavelength of the flow instability is restricted to being an integer fraction of the cell length, and a wavelength of one cell was observed where $\xi \leqslant 62.5\%$. Figure 23 shows the perturbation streamlines for $\xi = 66.75\%$ and 75%. In these cases the wavelength is one half of a cell, and the walls do not appear to interfere strongly with the perturbation wave. This decrease in wavelength is to be expected, as both the 'jet' width, and the width of the shear layers has decreased.

For each value of ξ the frequency of the instability was obtained from the velocity fluctuations at a point on the centreline. The wave speed was then obtained as the product of the wavelength and the frequency of the instability. Figure 24 shows a plot of the wave speed versus the baffle constriction ξ. Also shown on the plot are lines corresponding to the wave speed of the Tollmien–Schlichting wave for a wavelength equal to the baffle spacing and the velocity at the point of inflexion for the velocity profile midway between the baffles. As expected the wave speed tends towards the

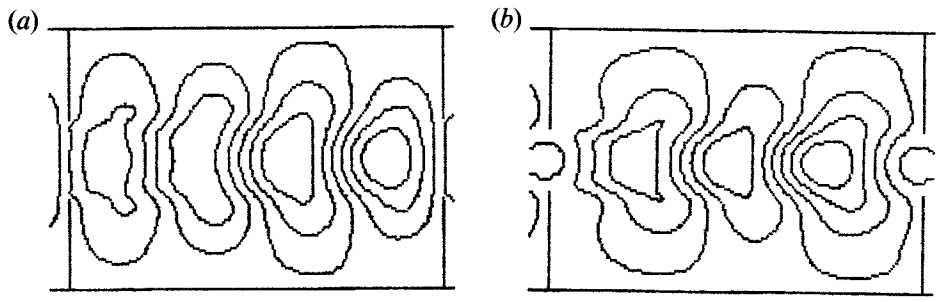

FIGURE 23. Instantaneous asymmetric perturbation streamlines, $Re = 200$. (a) $\xi = 66.75\%$. (b) $\xi = 75\%$.

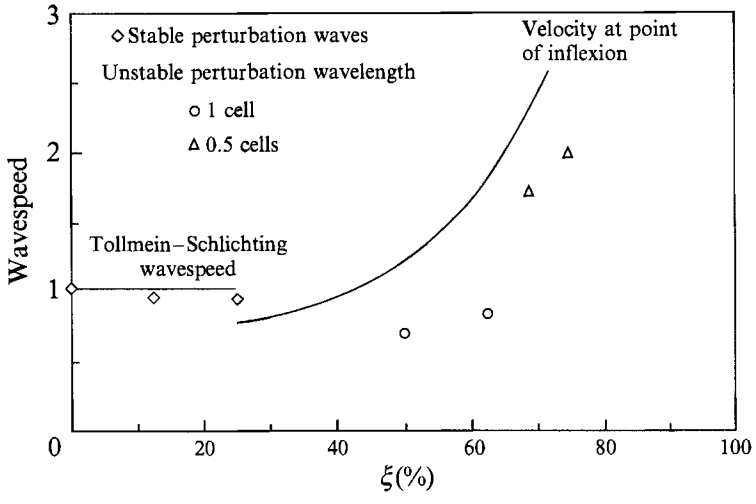

FIGURE 24. Velocity of the perturbation wave versus baffle constriction.

speed of the least stable Tollmien–Schlichting wave as ξ approaches 0%. As ξ becomes large the wave speed tends towards the velocity at the point of inflexion, though the presence of the walls appears to have considerably reduced the wave speed (Betchov & Criminale 1967).

From these observations the instability mechanism for the case studied in this paper ($\xi = 50\%$) would appear to be an inviscid instability associated with the shear layer. The frequency of the instability does not appear to be controlled by any simple mechanism, but is a complex interaction of the whole flow field. Viscous effects, the shear layer and the confining walls may all affect the wave speed of the instability, but the shear layer itself is thought to be primarily responsible for the transition to unsteadiness.

7. Discussion and conclusions

A numerical simulation has been successfully used to model two-dimensional incompressible Newtonian flow in baffled channels. The observed flows have been depicted using plots of the instantaneous streamlines, and these have been compared with experimental streakline photographs. Good agreement was observed between the

numerical simulation and the experimental flow visualization when the experimental flow was approximately two-dimensional.

For low-Reynolds-number ($Re < 100$) flow in baffled channels, a recirculating region was observed downstream of each baffle. With increasing Re the reattachment point was observed to move downstream until it became attached onto the downstream baffle. These flow patterns can be compared with the similar flows predicted by Rowley & Patankar (1984) for constant volumetric flow in baffled tubes. The flow patterns observed are also similar to flows observed in wavy walled channels (Sobey 1980), wavy walled tubes (Ralph 1986, 1987), and other similar geometries such as the sudden channel expansion (e.g. Sobey 1985).

At $Re \sim 100$ the flow was observed both numerically and experimentally to become unsteady and asymmetric. The experimental observations showed that this led to a secondary transition to three-dimensional turbulent flow. The baffles have therefore acted as a turbulence enhancement device leading to early transition, which will improve engineering properties such as heat transfer. Experimental data on heat transfer in baffled channels can be found in Kays & London (1964). This data shows that the baffles lead to a three-fold enhancement of the heat transfer coefficient, but at the expense of a three- to four-fold increase in pressure drop. Rowley & Patankar (1984) modelled heat transfer processes and predicted that the presence of periodic baffles in tubes would not provide efficient enhancement. They suggested that the slow moving recirculating regions effectively insulated the bulk of the fluid from the walls. The model used by Rowley & Patankar (1984) assumes the flow to be steady and axisymmetric up to $Re \sim 500$, contrary to experimental observations (Ni, private communication). Mackley, Tweddle & Wyatt (1990) observed that the presence of periodic baffles in a tube could lead to a dramatic enhancement in heat transfer for constant volumetric flows. A two-fold enhancement was found at Reynolds numbers as low as 300, contrary to the predictions of Rowley & Patankar (1984).

These observations indicate that the flow in complex geometries can become unsteady and turbulent at Reynolds numbers as low as 100. Engineering models commonly assume that the flow is steady or symmetric up to Reynolds numbers of order 1000, and this assumption should clearly not be taken for granted.

The successful modelling of early transition to turbulence in obstructed geometries may lead to an improved understanding of the operation of turbulent enhancement devices. If the mechanism for transition in this type of flow can be established then it may be possible to improve the design of turbulence enhancement devices. Karniadakis *et al.* (1988) demonstrated that in order to optimize the efficiency of such devices it was simply necessary to find the design that gave the minimum critical Reynolds number for transition to unsteady flow. However this calculation assumed that the increased energy loss associated with the obstruction is small. For severely constricted geometries such as the baffled channel the increase in energy loss owing to the presence of the baffles will clearly be significant, and the optimization of the geometry is more complex. An early transition to unsteady flow has commonly been observed in obstructed flows (e.g. eddy shedding from a cylinder), and this is normally associated with the presence of a shear layer. Rayleigh (1945) showed that a parallel flow with a point of inflexion in the velocity profile (this occurs in a shear layer) will be unstable in the inviscid limit. Conversely a flow with no point of inflexion can be shown to be stable in the inviscid limit. The presence of a shear layer appears to be critical for advancing transition. The object of geometric optimization should therefore be to obtain a sustained shear layer at a minimum Reynolds number with as little increase in energy loss as possible. Wire mesh inserts may well provide an excellent geometry

as each wire generates two shear layers which lead to an eddy shedding flow at low Reynolds number.

The experimental observation of the secondary transition to three-dimensional turbulence may have implications for transition processes in many similar geometries. The periodically cylindrically obstructed channel of Karniadakis *et al.* (1988), for example, was predicted to become unsteady at a Reynolds number of order 100, owing to a two-dimensional instability. It is likely that experimental observations or three-dimensional simulation of the flow in this geometry would show that this transition would be followed by a secondary instability to three-dimensional perturbations. This is similar to the mechanism for transition in plain channel flow observed experimentally at a Reynolds number of order 2000 (Orszag & Kells 1980).

The author is grateful to Dr M. R. Mackley and Dr N. E. Sherman for many valuable discussions, and to Professor T. J. Pedley for his suggestion that the flow might be treated as a confined jet. The project was carried out at the University of Cambridge Department of Chemical Engineering and was funded as a CASE award by BP Research and the SERC.

REFERENCES

AREF, H. 1984 Stirring by chaotic advection. *J. Fluid Mech.* **143**, 1.

BETCHOV, R. & CRIMINALE, W. O. 1967 *Stability of Parallel Flows.* Academic Press.

BRUNOLD, C. R., HUNNS, J. C. B., MACKLEY, M. R. & THOMPSON, J. W. 1989 Experimental observations on flow patterns and energy losses for oscillatory flow in ducts containing sharp edges. *Chem. Engng Sci.* **44**, 1227.

DRAZIN, P. G. & REID, W. H. 1981 *Hydronamic Stability.* Cambridge University Press.

DURST, F., MELLING, A. & WHITELAW, T. H. 1974 Low Reynolds number flow over a plane symmetrical sudden expansion. *J. Fluid Mech.* **64**, 111.

FEARN, R. M., MULLIN, T. & CLIFFE, K. A. 1989 Nonlinear flow phenomena in a symmetric sudden expansion. *J. Fluid Mech.* **211**, 595.

FORTIN, A., FORTIN, M. & GERVAIS, J. J. 1987 A numerical simulation of the transition to turbulence in a two dimensional flow. *J. Comput. Phys.* **70**, 295.

GHADDAR, N. K., KORZAK, K. Z., MIKIC, B. B. & PATERA, A. T. 1986 Numerical investigation of incompressible flow in grooved channels. Part 1. Stability and self-sustained oscillations. *J. Fluid Mech.* **163**, 99.

HO, E. M. & HUERRE, H. 1984 Perturbed free shear layers. *Ann. Rev. of Fluid Mech.* **16**, 365.

HOWES, T. 1988 Dispersion and unsteady flow in baffled tubes. PhD thesis, Department of Chemical Engineering, University of Cambridge.

HOWES, T., MACKLEY, M. R. & ROBERTS, E. P. L. 1991 The numerical simulation of chaotic mixing and dispersion for periodic flows in baffles channels. *Chem. Engng Sci.* **46**, 1669.

KAYS, W. M. & LONDON, A. L. 1964 *Compact Heat Exchangers*, 2nd edn. McGraw Hill.

KAO, T. W. & PARK, C. 1970 Experimental investigation of the stability of channel flows. Part 1. Flow of a single liquid in a rectangular channel. *J. Fluid Mech.* **43**, 145.

KARNIADAKIS, G. E., MIKIC, B. B. & PATERA, A. T. 1988 Minimum dissipation transport enhancement by flow destabilization: Reynolds analogy revisited. *J. Fluid Mech.* **192**, 365.

LIN, C. C. 1955 *The Theory of Hydrodynamic Stability.* Cambridge University Press.

MACKLEY, M. R. & SHERMAN, N. E. 1992 Cake filtration mechanisms in steady and unsteady flows. *Engineering of Membrane Processes, Bavaria, May 1992.*

MACKLEY, M. R., TWEDDLE, G. M. & WYATT, I. D. 1990 Experimental heat transfer measurements for pulsatile flow in a baffled tube. *Chem. Engng Sci.* **45**, 1237.

MILLS, R. D. 1968 Numerical solutions of viscous flow through a pipe orifice at low Reynolds numbers. *J. Mech. Engng Sci.* **10**, 133.

MOFFATT, H. K. 1964 Viscous and restricted eddies near a sharp corner. *J. Fluid Mech.* **18**, 1.

ORSZAG, S. A. 1971 Accurate solutions of the Orr Sommerfeld stability equation. *J. Fluid Mech.* **50**, 689.

ORSZAG, S. A. & KELLS, L. C. 1980 The transition to turbulence in plane Poiseuille flow and plane Couette flow. *J. Fluid Mech.* **96**, 159.

ORSZAG, S. A. & PATERA, A. T. 1983 Secondary stability of wall bounded shear flows. *J. Fluid Mech.* **128**, 347.

RALPH, M. E. 1986 Oscillatory flow in wavy walled tubes. *J. Fluid Mech.* **168**, 515.

RALPH, M. E. 1987 Steady flow structures and pressure drops in wavy walled tubes. *J. Fluids Engng* **109**, 255.

RALPH, M. E. & PEDLEY, T. J. 1988 Flow in a channel with amoving indentation. *J. Fluid Mech.* **190**, 87.

RAYLEIGH, J. W. S. 1945 *The Theory of Sound*, reprint of 2nd edn (first published 1896) Dover, New York.

ROACHE, P. J. 1976 *Computational Fluid Dynamics*. Hermosa, Albuquerque.

ROBERTS, E. P. L. 1992 *Unsteady Flow and Mixing in Baffled Channels*. PhD thesis, Department of Chemical Engineering, University of Cambridge.

ROWLEY, G. J. & PATANKAR, S. V. 1984 Analysis of laminar flow and heat transfer in tubes with internal circumferential fins. *Intl J. Heat Mass Transfer* **27**, 553.

SATO, H. 1961 Transition of a two dimensional jet. *J. Fluid Mech.* **7**, 53.

SOBEY, I. J. 1980 On flow through furrowed channels. Part 1. Calculated flow patterns. *J. Fluid Mech.* **96**, 1.

SOBEY, I. J. 1985 Observation of waves during oscillatory channel flow. *J. Fluid Mech.* **151**, 395.

SOBEY, I. J. & DRAZIN, P. G. 1986 Bifurcations of two-dimensional channel flows. *J. Fluid Mech.* **171**, 263.

SREENIVASAN, F. R. & STRYKOWSKI, P. T. 1987 An instability associated with a sudden pipe expansion. *Phys. Fluids* **26**, 2766.

THOMPSON, J. M. T. & STEWART, H. B. 1986 *Nonlinear Dynamics and Chaos*. Wiley.

WHITE, F. M. 1974 *Viscous Fluid Flow*. McGraw Hill.